Electron. Mater. Lett., Vol. 13, No. 4 (2017), pp. 318-323
DOI: 10.1007/s13391-017-6289-0

Triboelectric Charge Generation by Semiconducting SnO_2 Film Grown by Atomic Layer Deposition

No Ho Lee[1], Seong Yu Yoon[1], Dong Ha Kim[1], Seong Keun Kim[2], and Byung Joon Choi[1,*]

[1]Department of Materials Science and Engineering, Seoul National University of Science and Technology, Seoul 01811, Korea
[2]Center for Electronic Materials, Korea Institute of Science and Technology, Seoul 02792, Korea

(received date: 1 September 2016 / accepted date: 3 February 2017 / published date: 10 July 2017)

Improving the energy harvesting efficiency of triboelectric generators (TEGs) requires exploring new types of materials that can be used, and understanding their properties. In this study, we have investigated semiconducting SnO_2 thin films as friction layers in TEGs, which has not been explored thus far. Thin films of SnO_2 with various thicknesses were grown by atomic layer deposition on Si substrates. Either polymer or glass was used as counter friction layers. Vertical contact/separation mode was utilized to evaluate the TEG efficiency. The results indicate that an increase in the SnO_2 film thickness from 5 to 25 nm enhances the triboelectric output voltage of the TEG. Insertion of a 400-nm-thick Pt sub-layer between the SnO_2 film and Si substrate further increased the output voltage up to ~120 V in a 2 cm × 2 cm contact area, while the enhancement was cancelled out by inserting a 10-nm-thick insulating Al_2O_3 film between SnO_2 and Pt films. These results indicate that *n*-type semiconducting SnO_2 films can provide triboelectric charge to counter-friction layers in TEGs.

Keywords: triboelectric generator, semiconductor, SnO_2, sub-layer

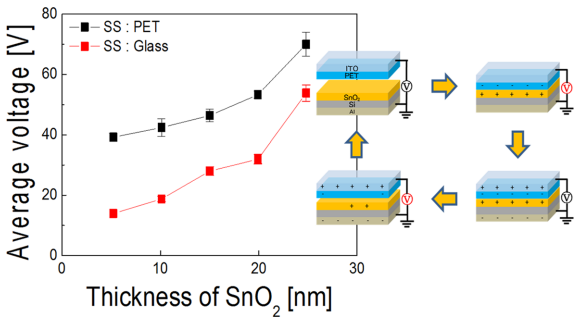

1. INTRODUCTION

There has been ever-increasing interest in energy harvesters that recover waste energy from the environment, for use as power sources for self-powered electronic equipment or as supporters for their battery systems.[1] Triboelectric generators (TEGs) are among the various types of energy harvesters under investigation for such systems. These convert the mechanical frictional energy of the system into electrical energy via creation of electrostatic charge on the surfaces of two dissimilar materials when they are in physical contact. Such contact-induced triboelectric charge can generate a potential drop when the two surfaces are separated by a mechanical force. Therefore, electrons will flow between two electrodes connected to opposite surfaces of the two material specimens, until the potential drop has diminished. Any mechanical energy that is wasted in our daily life, such as walking and other types of human movements, vibrations, mechanical triggers, rotating tires, wind, and flowing water can be used for generation of electricity through this method.[2]

In addition to such a broad range of applications, TEGs have attracted a great deal of attention recently owing to their simple operating principle, high power density, and high energy conversion efficiency, and the ease in selecting materials to fabricate them.[3-12] Different types of mechanical motions and structures have been employed for fabrication of prototype TEGs, including vertical contact/separation mode, in-plane sliding mode, single-electrode mode, and

*Corresponding author: bjchoi@seoultech.ac.kr

free-standing triboelectric-layer mode.[3-5,9,11,12] Most of the friction layers used for TEGs thus far are polymeric dielectrics or noble metal islands on polymer surfaces. Various kind of polymeric materials have been reported as friction layers for TEG applications, such as PDMS (Polydimethylsiloxane), PET (Polyethylene terephthalate), KAPTON (polyimide film developed by DuPont), and PTFE (Polytetrafluoroethylene).[3,4,7,8,11] However, triboelectric properties of semiconducting materials have not been studied in detail.

In this study, we have used semiconducting SnO_2 thin films as a friction layer in TEGs. Usually polymers tend to degrade due to humidity, heat, mechanical friction, and chemical agents that are present in typical environments in which TEGs operate. In contrast, SnO_2 films have good chemical and mechanical stability compared to polymers, and therefore it is expected that the lifetime of a TEG with a SnO_2 film will be enhanced.[13]

In this work, the SnO_2 thin films were grown by atomic layer deposition (ALD). ALD can control the film thicknesses in the sub-nanometer scale. This is useful in evaluating the dependence of triboelectricity of the friction layer by its thickness and electron affinity. In addition, ALD can grow conformal thin films even on a transferred pattern, and it can preserve complicated surface structures on the sub-layer, such as pyramids, cubes, and other rough surface features that increase friction efficiency.[9,14,15]

Previously, we have reported that SnO_2 friction layers act as the positive side in the triboelectric series when vertically contacted with PET and glass.[3] It is believed that free electrons in an *n*-type semiconducting SnO_2 friction layer may be transferred to an opposing friction layer that tends to accept electrons. Based on this, it is evident that SnO_2 must be placed ahead of polymer and glass materials in the triboelectric series.

In this study, we tested the triboelectric property of various SnO_2 films with different thicknesses and sub-layers. When the thicker SnO_2 layer was vertically contacted with PET or glass, higher output voltages were generated. A Pt sub-layer under SnO_2 could enhance the triboelectric output voltage, while Al_2O_3 inserted between Pt and SnO_2 layers screened out the effect of Pt sub-layer. These phenomena were explained by taking into consideration the energy levels of the friction layers and sub-layers.

2. EXPERIMENT PROCEDURE

Cross sectional schematic diagrams of the samples produced in this study are presented in Fig. 1. They are denoted as SnO_2, glass, or PET depending on the friction layer. The SnO_2 thin films were grown by ALD on bare *p*-type Si wafers. TDMA-Sn (Tetrakis(dimethylamino)tin) and water were used as the metalorganic precursor and oxidant, respectively, at a wafer temperature of 200 °C. To investigate the effect of the film thickness, SnO_2 thin films with various thicknesses from 5 nm to 25 nm were deposited. The thicknesses of the thin films were measured by spectroscopic ellipsometry (SE). A conducting aluminum tape was attached to the backside of the silicon substrate for extracting the triboelectric charge.

For the investigating the influence of the sub-layer on the triboelectric effect of the semiconducting SnO_2 films, we first introduced a Pt film as an electron supplying layer under the SnO_2 film, and then, introduced an insulating Al_2O_3 film

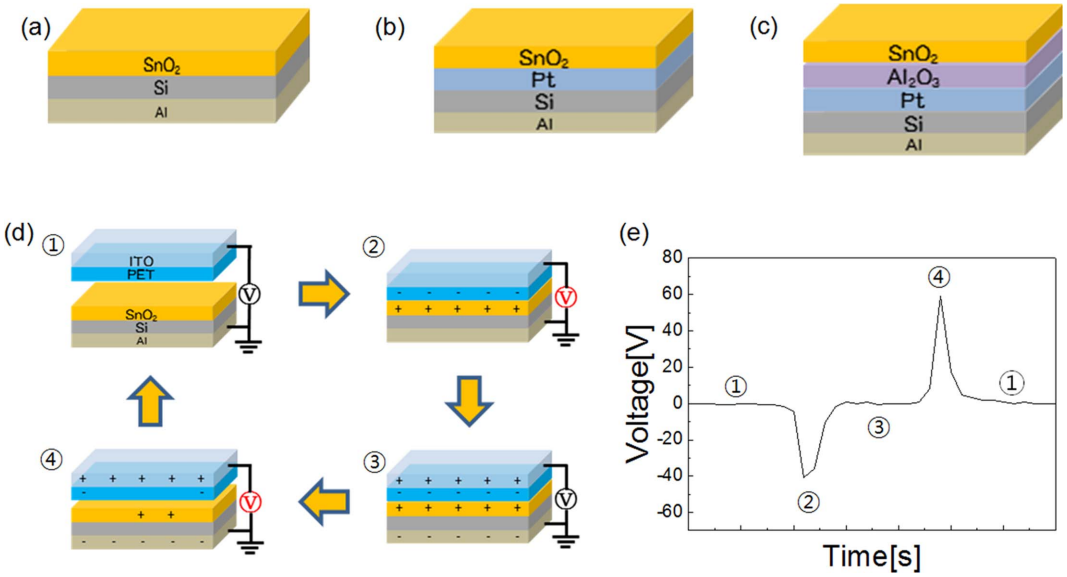

Fig. 1. Schematics of the samples and the charge generation in triboelectric generator (TEG). (a) SnO_2 on Si with Al electrode (SS), (b) SnO_2/Pt/Si/Al (SPS), (c) SnO_2/Al_2O_3/Pt/Si/Al (SAPS), (d) Illustration of TEG working and (e) output voltage trace one by one.

as an electron shielding layer between the SnO_2 and Pt films; the schematics of these samples are shown in Figs. 1(b) and (c), respectively. For the sample depicted in Fig. 1(b), a 400-nm-thick Pt layer was deposited by electron-beam evaporation on a bare Si wafer. For the sample in Fig. 1(c), the 10 nm of Al_2O_3 film between the SnO_2 and Pt was deposited by ALD using trimethyl aluminum (TMA) and water. Al conducting tape was attached to the lower side of the silicon substrate to act as the electrical contact. The samples with SnO_2/Si, SnO_2/Pt/Si, and SnO_2/Al_2O_3/Pt/Si stacks are denoted as SS, SPS, and SAPS, respectively. As counter-friction layers against the SnO_2 films, 0.7 mm-thick glass (Corning) on FTO (Fluorine-doped tin oxide) and 0.127 mm-thick PET (Sigma Aldrich) on ITO (In doped tin oxide) electrodes were used.

In order to induce mechanical friction, the two friction layers consisting of SnO_2 and glass or PET were brought in contact vertically, and subsequently separated by means of a stepping motor. One segment was attached to the lower ground surface, and the other was securely attached to the upper side of the arm of the stepping motor. The two segments could be contacted and separated by the motion of the stepping motor back and forth with 45 ° of rotation angle at a speed of 0.134 m/s.[3]

The sequential engagement of mechanical contact, followed by separation and the corresponding TEG output voltage is presented in Figs. 1(d) and (e). When the two segments are in contact, triboelectric charge is transferred from one friction layer to the other. This charge transfer induces an electrostatic field between the electrodes and free electrons flow through the external circuit. When the two samples are separated, an electrical potential difference is generated between two electrodes. To compensate this potential difference, electrons flow backwards. The output voltage generated by periodic contact and separation of the two segments can be measured by an oscilloscope.[9,16] All the measurements were performed at atmospheric pressure and room temperature.

3. RESULTS AND DISCUSSION

The output voltage measured when the SS and PET segments were brought in contact and separated repeatedly is shown in Fig. 2. Figure 2(a) shows the waveforms of output voltage in the different SS samples with SnO_2 thickness of 10, 15, and 25 nm. With increasing SnO_2 thickness, a higher output voltage was observed. Figure 2(b) shows the average output voltage as a function of SnO_2 thickness with a counter-friction layer of glass or PET. The output voltage was averaged by taking the highest three peaks for each sample among dozens of vertical contact/separation cycles. Based on the height and polarity of the

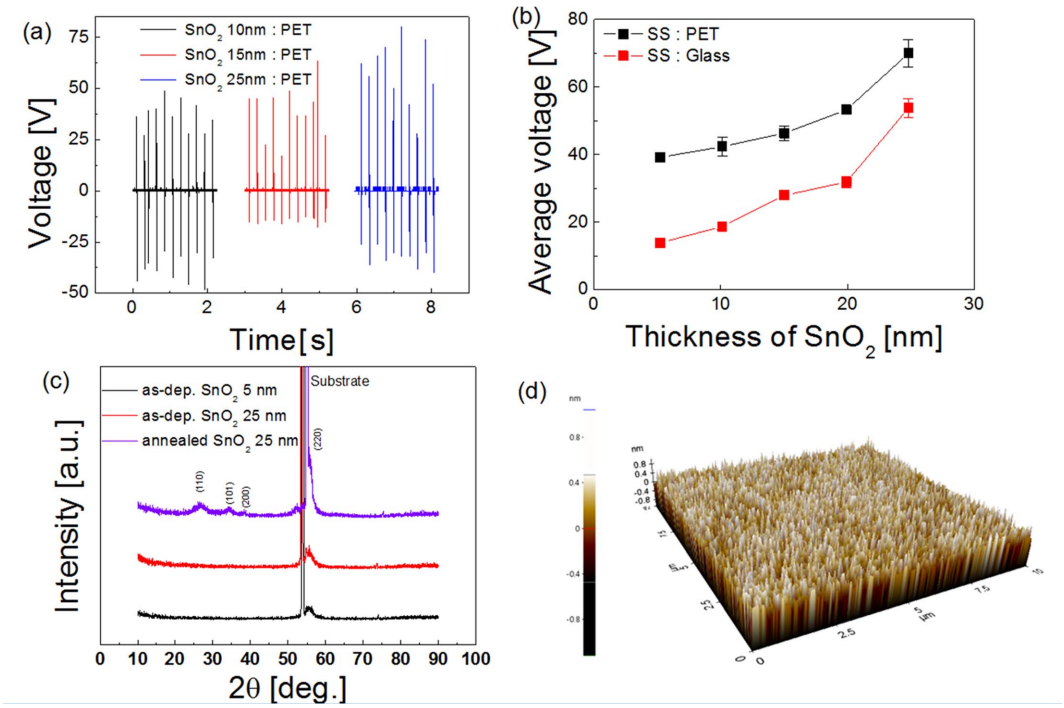

Fig. 2. (a) Output voltage traces of the SS TEGs in the variation of SnO_2 thickness of 10, 15, 25 nm, respectively. (b) Average output voltage as a function of the SnO_2 thin film thickness with the counter-friction layer materials of glass and PET. (c) XRD spectra of as-deposited SnO_2 thin film on Si by 5 nm and 25 nm, and that of 25-nm-thick SnO_2 on Si annealed at 400 °C in air. (d) Surface morphology of 25-nm-thick as-grown SnO_2 film on Si gained by AFM measurement.

TEG output voltage, the triboelectric series was determined as SnO_2 – glass – PET, where SnO_2 is in the positive side, which means that PET can accept more charge from SnO_2 than the combinations glass-PET or glass-SnO_2.[3]

To determine the reason behind the thickness effect of the SnO_2 film, physical characteristics of SnO_2 films with SS stacks were analyzed. Figure 2(c) shows X-ray diffraction (XRD) patterns of the as-deposited SnO_2 thin films on Si wafers with the thickness of 5 nm and 25 nm, respectively. The as-deposited SnO_2 films are amorphous as indicated by XRD, and no obvious difference in crystallinity was observed among the films with different thicknesses. For comparison, the XRD pattern of a 25-nm-thick SnO_2 film annealed at 400 °C shows peaks corresponding to a crystalline film. The crystallized SnO_2 film slightly enhances the output voltage of the TEG.

Atomic force microscopy (AFM) measurements were also carried out. Figure 2(d) shows the surface morphology of 25-nm-thick SnO_2 film on Si. The R_{rms} (root-mean-squared roughness) and R_a (average roughness) values are 0.24 nm and 0.192 nm, respectively. R_{rms} is the standard deviation of the height in a specific region of the surface, and R_a is the average surface height with respect to the center plane.[17] Roughness of an ALD-grown 25-nm-thick SnO_2 film is almost identical as that of the bare Si substrate. These physical characteristics imply that the surface of the SnO_2 for both thin and thick films are amorphous and very flat, and therefore, the crystallinity and surface roughness are not responsible for the variation in the output voltage as a function of the thickness of the SnO_2 films.

One can expect thicker SnO_2 films to have higher charge density, which could result in an increased electric field and larger potential difference across the SnO_2 film according to Poisson's equation. In this regard, it is understood that greater amounts of electron and oxygen vacancies are generated in thicker SnO_2 films, and those free electrons can be transferred to the counter-friction layer once the two friction layers are brought into contact. When they are separated, charge density due to the remaining oxygen vacancies in the SnO_2 film can generate an internal electric field and potential difference, which induces a reverse current flow. Therefore, the integrated charge density and electric field in the SnO_2 films will determine the TEG output voltage.

To glean further insight into the charge density effect on the TEG output voltage, samples with stacks of SS, SPS, and SAPS were systematically investigated. Note that the Pt sub-layer is floating on the Si or Al_2O_3/Si substrate meaning that Al back-contact electrode is grounded. The thickness of the SnO_2 friction layer was fixed at 10 nm. The waveform and output voltage measured from several samples are shown in Fig. 3. Here, the counter-friction layer in all measurements was PET. Figure 3(a) shows how the TEG output voltage changes depending on the type of sub-layer under SnO_2. As shown in Fig. 3(b), the average output voltage of the TEG was greatly increased when the Pt film was introduced under the SnO_2 layer in SPS. However, when the 10-nm-thick Al_2O_3 film was inserted between the Pt and SnO_2 films in SAPS, the output voltage decreased to a level comparable to that of SS. Slightly higher output voltage of SAPS than that of SS could be explained by the larger variation in the output voltage owing to the rough surface on top of 400 nm-thick Pt sub-layer.

Based on the influence of the SnO_2 thickness and type of sub-layer, it is possible to conclude that the amount of electrons transferred from SnO_2 to the counter-friction layer determines the output voltage. More electrons can be transferred from SnO_2 with increasing thickness from 5 to 25 nm. When a Pt film is inserted under the SnO_2 film, it may provide more free electrons to the SnO_2 layer. Therefore, the SnO_2 film can subsequently donate more triboelectric charge to the counter-friction layer. This means that a greater electrostatic field and electric potential difference between the two electrodes is generated, which results in an increase in the TEG output voltage. On the other hand, a layer of Al_2O_3 inserted between the Pt and SnO_2 films hinders electron transfer from Pt to SnO_2, since Al_2O_3 is known to be a good insulating dielectric material.[18] This hypothesis is

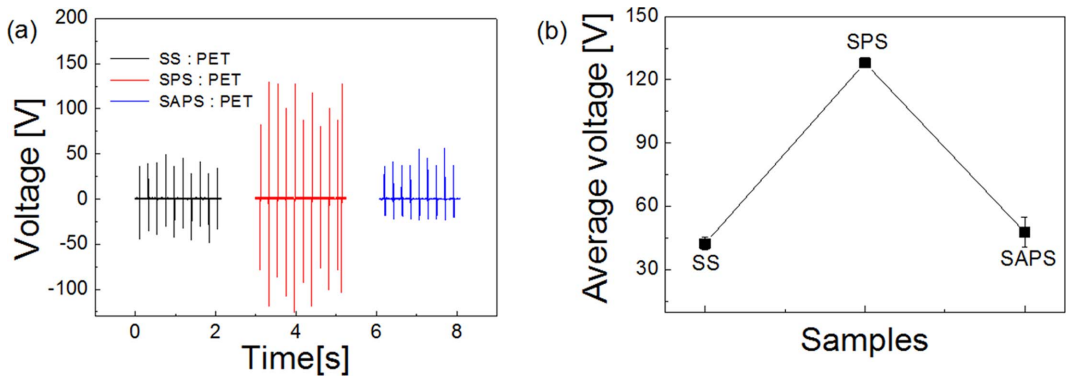

Fig. 3. (a) Output voltage traces of various TEGs (SS, SPS, and SAPS) with PET, (b) Average output voltage of TEGs with the sub-layers.

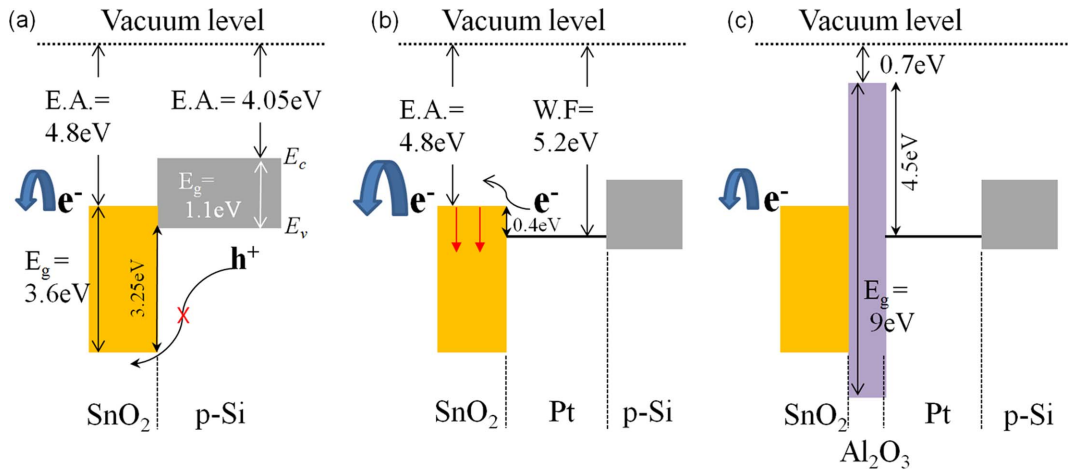

Fig. 4. Energy band diagram of TEGs depending on the sub-layers. (a) SS, (b) SPS, and (c) SAPS.

further supported by considering the energy band diagrams of the materials, as discussed below.

Figures 4(a)-(c) show the energy band diagrams of SS, SPS, and SAPS, respectively. When SnO_2 films are grown directly on Si, as shown in Fig. 4(a), there is no electron donation from the *p*-Si substrate. On the other hand, holes in the valance band of *p*-Si cannot cross over to the SnO_2 because hole barrier height is too high (3.25 eV expected).[19] Therefore, only the surplus electrons from SnO_2 can be transferred to the counter-friction layer.

When Pt is introduced under the SnO_2 layer, SnO_2 can get extra electrons from the Pt sub-layer due to the relatively low energy barrier between Pt and SnO_2 (< 0.4 eV expected), as shown in Fig. 4(b).[19] Moreover, sufficient band edge states near conduction minimum band in amorphous SnO_2 may enable the facile injection of electrons.[20] However, when Al_2O_3 is present between SnO_2 and Pt, there is no electron donation from Pt due to the large band gap of Al_2O_3 as shown in Fig. 4(c).[18] Highly insulating Al_2O_3 prevents electron transfer from Pt to SnO_2.

As mentioned earlier, SnO_2 is an intrinsic *n*-type semiconductor that is apt to generate surplus electrons via oxygen vacancies.[21] This property has allowed the use of SnO_2 as a semiconductor-type gas sensor.[3,22-26] We believe that the SnO_2 friction layers in this study can easily donate these surplus electrons to the counter-friction layer. The thickness effect can be explained based on the number of electrons that can be transferred. Increasing the thickness of the SnO_2 film results in a larger number of oxygen vacancies that can contribute to an increase in the number of electrons.[21] When a Pt sub-layer is introduced under the SnO_2, it can provide even more electrons. Facile charge injection that overcomes the barrier between Pt and SnO_2 can be explained by taking several factors into consideration. The thin SnO_2 films deposited via ALD are amorphous, which results in a large number of defects at the Pt/SnO_2 interface. These imperfections create additional energy levels in the band structure of SnO_2, allowing electron transfer between the two materials. In addition, the removal of electrons from SnO_2 lowers the Fermi level,[11] further facilitating the transfer of electrons from Pt to SnO_2 (Fig. 4(b)).

Power efficiency of TEGs with semiconducting SnO_2 was compared with those reported in literature. In the case of SPS contacted with PET, we obtained a peak output voltage, current density and power density of ~125 V, ~2.75 μA/cm^2, and ~0.344 mW/cm^2, respectively, with a 4 cm^2 contact area. Here, the current density is estimated from the equation of $I = C \times (dV/dt)$, where C means the series capacitance of two contacted TEG samples (e.g. SPS:PET). Jung *et al.* recently reported a piezo/triboelectric hybrid generator and ~370 V of output voltage, ~12 μA/cm^2 of current density, and ~4.44 mW/cm^2 of power density with a contact area of 21 cm^2.[12] Wang *et al.* reported an output voltage of ~1300 V, a short-circuit current density of ~0.41 μA/cm^2 and a peak power density of ~0.53 mW/cm^2 with a 35.5 cm^2 area of sliding-mode TEG.[5] Although the output voltage in some of our SnO_2-PET TEGs is relatively low (probably due to the small area) the current density and power density are comparable than those of others in the aforementioned studies. It is worth noting that since ALD-grown SnO_2 can be applied to techniques that involve complicated patterns or hybridization with piezoelectric generators, power efficiency could potentially be enhanced further.

4. CONCLUSIONS

Output voltages of TEGs composed of SnO_2 semiconducting thin films as the friction layers were evaluated in vertical contact/separation mode. It was observed that the thicknesses of the ALD-grown SnO_2 films and the type of sub-layer influence the TEG output voltage. The thicker the SnO_2 film,

the higher the TEG output voltage that was generated. The presence of a Pt sub-layer under the SnO_2 film enhanced the TEG output voltage, while insertion of an Al_2O_3 film between SnO_2 and Pt cancelled out the enhancement of output voltage. From these results, it was concluded that the combination of a thicker SnO_2 film and a Pt sub-layer provide maximum triboelectric charge to a counter-friction layer composed of PET or glass. The facile charge injection observed for this configuration is attributed to the low energy barrier between the materials and imperfections at the Pt/SnO_2 interface. The results of our work are expected to motivate and facilitate further studies on materials and mechanisms relating to the triboelectric effect, with the aim to enhance the power efficiency and robustness of TEG systems.

ACKNOWLEDGMENT

This research was supported by Basic Science Research Program through the National Research Foundation of Korea (NRF) funded by the Ministry of Education (2014R1A1A2054597).

REFERENCES

1. A. A. A. Rahman, W. A. W. Jamil, and A. A. Umar, *Electron. Mater. Lett.* **12**, 545 (2016).
2. Z. L. Wang, J. Chen, and L. Lin, *Energy Environ. Sci.* **8**, 2250 (2015).
3. N. H. Lee, J. R. Shin, J. E. Yoo, D. H. You, B.-R. Koo, S. W. Lee, H.-J. Ahn, and B. J. Choi, *J. Korean Powder Metall. Inst.* **22**, 321 (2015).
4. W. Yang, J. Chen, G. Zhu, X. Wen, P. Bai, Y. Su, Y. Lin, and Z. Wang, *Nano Res.* **6**, 880 (2013).
5. S. Wang, L. Lin, Y. Xie, Q. Jing, S. Niu, and Z. L. Wang, *Nano Lett.* **13**, 2226 (2013).
6. Z. L. Wang, G. Zhu, Y. Yang, S. Wang, and C. Pan, *Mater. Today* **15**, 532 (2012).
7. Y. H. Ko, G. Nagaraju, S. H. Lee, and J. S. Yu, *ACS Appl. Mater. Interfaces* **6**, 6631 (2014).
8. Y. Yang, H. Zhang, Z. H. Lin, Y. S. Zhou, Q. Jing, Y. Su, J. Yang, J. Chen, C. Hu, and Z. L. Wang, *ACS Nano* **7**, 9213 (2013).
9. F.-R. R. Fan, L. Lin, G. Zhu, W. Wu, R. Zhang, and Z. L. Wang, *Nano Lett.* **12**, 3109 (2012).
10. A. F. Diaz and R. M. Felix-Navarro, *J. Electrostat.* **62**, 277 (2004).
11. X. S. Meng, Z. L. Wang, and G. Zhu, *Adv. Mater.* **28**, 668 (2015).
12. W.-S. Jung, M.-G. Kang, H. G. Moon, S.-H. Baek, S.-J. Yoon, Z.-L. Wang, S.-W. Kim, and C.-Y. Kang, *Sci. Rep.* **5**, 9309 (2015).
13. H. S. Lee and S. I. Woo, *Electron. Mater. Lett*. **12**, 499 (2016).
14. S. M. George, *Chem. Rev.* **110**, 111 (2010).
15. J. Heo, A. S. Hock, and R. G. Gordon, *Chem. Mater.* **22**, 4964 (2010).
16. F.-R. Fan, Z.-Q. Tian, and Z. Lin Wang, *Nano Energy* **1**, 328 (2012).
17. B.-R. Koo and H.-J. Ahn, *Ceram. Int.* **42**, 509 (2016).
18. N. Satoh, I. Cesar, M. Lamers, I. Romijn, K. Bakker, C. Olson, D. O. Saynova, Y. Komatsu, A. Weeber, F. Verbakel, and M. Wiggers, *e-J. Surf. Sci. Nanotech.* **10**, 22 (2012).
19. K. Hwang, J.-S. Yeo, S.-S. Kim, D.-Y. Kim, and S.-I. Na, *Semicond. Sci. Technol.* **30**, 015014 (2015).
20. R. A. Street and N. F. Mott, *Phys. Rev. Lett.* **35**, 1293 (1975).
21. M. Utriainen, K. Kovács, J. M. Campbell, L. Niinistö, and F. Réti, *J. Elctrochemical Soc.* **146**, 189 (1999).
22. W.-S. Choi, *Trans. Electr. Electron. Mater.* **10**, 200 (2009).
23. C.-W. Cho, J.-H. Lee, D.-H. Riu, and C.-Y. Kim, *Jpn. J. Appl. Phys.* **51**, 045001 (2012).
24. Y.-J. Choi, I.-S. Hwang, J.-G. Park, K. J. Choi, J.-H. Park, and J.-H. Lee, *Nanotechnology* **19**, 095508 (2008).
25. M. Kanamori, K. Suzuki, Y. Ohya, and Y. Takahashi, *Jpn. J. Appl. Phys.* **33**, 6680 (1994).
26. P. Grosse, F. J. Schmitte, G. Frank, and H. Köstlin, *Thin Solid Films* **90**, 309 (1982).